

THEORETICAL AND EXPERIMENTAL STUDY OF MICRO-CRACKING INDUCED BY THE RAYLEIGH WAVE

J. F. CARDENAS-GARCIA and D. C. HOLLOWAY

*Department of Mechanical Engineering
University of Maryland
College Park, MD 20742*

Abstract

This paper examines the extension of surface micro-cracks induced by a surface or Rayleigh wave (R-wave). This problem is examined both theoretically and experimentally. The theoretical approach involves a full-field reappraisal of the Lamb solution for a surface wave propagating in a homogeneous, isotropic, elastic, two-dimensional material, for the cases of plane strain and plane stress. Using the Griffith-Irwin energy release rate fracture criterion for cracks under combined Mode I and Mode II loading, a prediction is made of the path and final length of the surface micro-crack extension produced by the R-wave. Predictions of the crack extension direction are also obtained using the maximum normal stress fracture criterion. The experimental approach uses dynamic photoelasticity to observe the isochromatic patterns associated with a R-wave propagating along the narrow edge of a transparent, birefringent plate, examining in detail the process of crack extension. When the theoretically and experimentally obtained results are compared, reasonable agreement is obtained.

Introduction

A previous paper [1] dealt with a detailed appraisal of the solution by Rayleigh for the surface wave phenomena that bears his name. This theoretical appraisal led to a hypothesis for the initiation and propagation of cracks by the passage of a Rayleigh wave (R-wave). The hypothesis was verified experimentally using large plates of glass and Homalite 100. This paper deals with a parallel appraisal of surface waves, using the Lamb solution [2], but following the treatment of Dally and Thau [3, 4], which considers the entire field of the R-wave. Both plane strain and plane stress solutions of the R-wave generated by a line load applied to a semi-infinite body have been examined.

The expressions for the characteristic or Rayleigh equation, the displacements, and the stresses over the full-field have been derived. Detailed numerical calculations have been

carried out and computer-generated isochromatic plots have been obtained which compare quite favorably to those observed experimentally. In addition, calculations of the cumulative strain energy contained in the R-wave field have been made, which confirm that a large portion of the energy contained in a propagating R-wave lies within one wavelength depth into the medium. Finally, the maximum normal stress fracture criterion [5] is used to obtain estimates of the crack extension direction, and crack extension is predicted using the Griffith-Irwin strain energy release rate fracture criterion [6, 7].

The model

The geometry considered is shown in Figure 1. Examination of the boundary conditions yields the Rayleigh equation:

$$(K_1^2)^3 - 8(K_1^2)^2 + (24 - 16\alpha_1^2)(K_1^2) + (16\alpha_1^2 - 16) = 0 \quad (1)$$

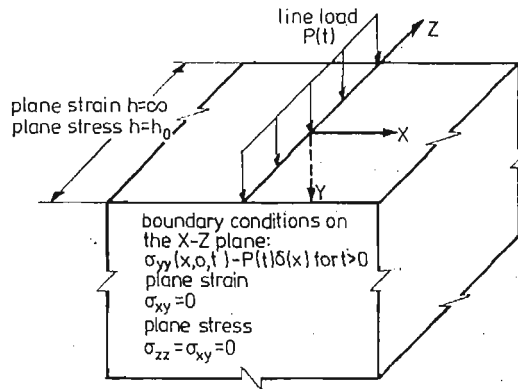


Fig. 1. Geometry of the semi-infinite plate used for the Lamb solution

where for plane strain

$$\alpha_1^2 = \frac{1-2\nu}{2(1-\nu)} = \left(\frac{k_l}{k_t}\right)^2 = \left(\frac{C_2}{C_1}\right)^2 \quad (2)$$

and

$$K_1^2 = \left(\frac{k_t}{k_R}\right)^2 = \left(\frac{\omega}{k_R C_2}\right)^2 = \left(\frac{C_R}{C_2}\right)^2 \quad (3)$$

and for plane stress (where α_1 and K_1 change to α_p and K_p , respectively),

$$\alpha_p^2 = \frac{(1-\nu)}{2} = \left(\frac{k_p}{k_t}\right)^2 = \left(\frac{C_2}{C_p}\right)^2 \quad (4)$$

and

$$K_p^2 = \left(\frac{k_t}{k_E}\right)^2 = \left(\frac{\omega}{K_E C_2}\right)^2 = \left(\frac{C_E}{C_2}\right)^2 \quad (5)$$

where k_l , k_p , k_t , k_R and k_E are the wave numbers associated with the various waves. C_E represents the R-wave velocity in plane stress. The Rayleigh equation shows that the

R-wave velocity, C_R or C_E , is independent of wave frequency and dependent only on the elastic properties of the material.

The equations for the plane strain displacements are:

$$u = k[\Phi'(\zeta_1) - \frac{2qs}{(s^2+k^2)}\Phi'(\zeta_2)], \quad (6)$$

$$v = iq[\Phi'(\zeta_1) - \frac{2k^2}{(s^2+k^2)}\Phi'(\zeta_2)], \quad (7)$$

$$w = 0 \quad (8)$$

where,

$$\mu\Phi'(\zeta_j) = \frac{i\lambda_1 A}{[4\pi(s^2-q^2)]} \sum_{n=1}^4 B_n(\zeta_j-t_n)^2 \ln(\zeta_j-t_n) \quad (9)$$

for $j = 1, 2$. q and s are the dilatational and distortional wave attenuation factors, respectively. The equations for the plane stress displacements are obtained by changing q to r , where r now represents the plate wave attenuation factor. The displacement in the z -direction, w , is non-zero for plane stress, but for the current analysis is unimportant.

The equations for the plane strain stresses are:

$$\sigma_{xx} = -\mu[(s^2-2q^2-k^2)\Phi''(\zeta_1) + (s^2+k^2)\Phi''(\zeta_2)], \quad (10)$$

$$\sigma_{yy} = -\mu(s^2+k^2)[\Phi''(\zeta_1) - \Phi''(\zeta_2)], \quad (11)$$

$$\sigma_{zz} = -\mu(s^2-2q^2+k^2)\Phi''(\zeta_1), \quad (12)$$

$$\sigma_{xy} = i2\mu q k[\Phi''(\zeta_1) - \Phi''(\zeta_2)], \quad (13)$$

$$\sigma_{yz} = \sigma_{zx} = 0, \quad (14)$$

where,

$$\mu\Phi''(\zeta_j) = \frac{i\lambda_1 A}{[2\pi(s^2-q^2)]} \sum_{n=1}^4 B_n(\zeta_j-t_n) \ln(\zeta_j-t_n) \quad (15)$$

for $j = 1, 2$.

The stress equations for the plane stress solution can be obtained by setting or changing parameters as follows:

$$\sigma_{zz} = 0 \quad (16)$$

$$q \rightarrow r, \quad k \rightarrow k_E. \quad (17)$$

The isochromatics can be calculated using the stress-optic law:

$$2\tau_{max} = \sigma_1 - \sigma_2 = \frac{f_\sigma}{h} N \quad (18)$$

where h is the thickness of the model, N is the fringe or isochromatic order, and f_σ is the material fringe value. This law, for a two-dimensional material, indicates that the stress difference ($\sigma_1 - \sigma_2$) can be determined if the fringe order N can be measured and if the material fringe value f_σ can be established by means of calibration. This can be done using a plane polariscope. It is also possible to do the inverse, that is to determine the

fringe order knowing the principal stress difference, the thickness of the plate and the material fringe value. It is then possible to obtain a fullfield view of the surface wave using isochromatics.

The strain energy per unit volume or strain energy density, U_0 , for plane strain, is given by:

$$U_0 = \frac{1}{2E} (\sigma_{xx}^2 + \sigma_{yy}^2 + \sigma_{zz}^2) - \frac{\nu}{E} (\sigma_{xx}\sigma_{yy} + \sigma_{yy}\sigma_{zz} + \sigma_{xx}\sigma_{zz}) + \frac{1}{2\mu} \sigma_{xy}^2. \quad (20)$$

For plane stress, it is given by:

$$U_0 = \frac{1}{2E} (\sigma_{xx}^2 + \sigma_{yy}^2) - \frac{\nu}{E} \sigma_{xx}\sigma_{yy} + \frac{1}{2\mu} \sigma_{xy}^2, \quad (21)$$

which implies that the strain energy can be expressed as:

$$U = \int_0^{y_0} \int_0^l \int_0^h U_0 dz dx dy = h \int_0^{y_0} \int_0^l U_0 dx dy \quad (22)$$

where h is the thickness of the material in which the plane R-wave travels.

Figure 2 shows the normalized strain energy plotted against normalized depth for plane strain and plane stress. The normalized strain energy represents that portion, up

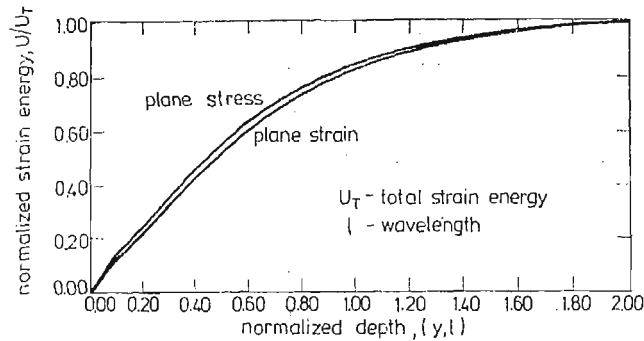


Fig. 2. The Lamb solution — normalized cumulative strain energy as a function of normalized depth, for plane strain and plane stress, $\nu = 0.35$

to a depth y_0 ($0 \leq y_0 \leq 2e$), of the total strain energy per unit width contained in a R-wave which is one wavelength (e) long and two wavelengths deep. More of the strain energy associated with the plane stress solution lies close to the surface than that of the plane strain solution. Or, at a given normalized depth, the plane stress solution shows a greater relative amount of cumulative strain energy than the plane strain solution. Even so, more than 80% of the strain energy is contained within one wavelength from the surface for both cases.

Figure 3 shows a representation of the magnitudes and directions, on and below the surface, of the principal stresses associated with a R-wave. The R-wave is moving to the right and the principal stresses have been normalized with respect to the largest principal stress occurring at the surface. The larger principal stress, σ_1 , at any particular point is represented by solid lines and the smaller principal stress, σ_2 , is represented by dotted

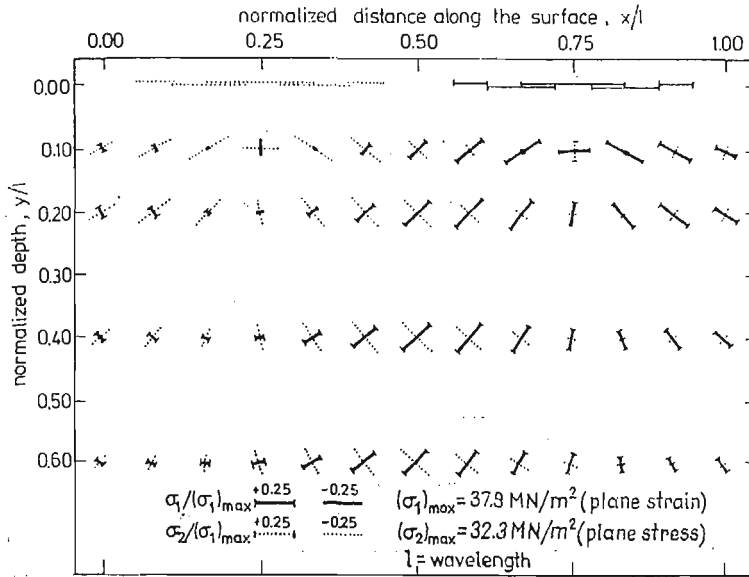


Fig. 3. The Lamb solution — normalized principal stresses and directions on and below the surface for plane strain and plane stress, $\nu = 0.35$.

lines. If a stress is positive a small bar is attached at each end of the respective representation of stress and if it is negative, no bar is added. The first half-wavelength of the R-wave, at the surface, exhibits a tensile component while the second half-wavelength of the R-wave exhibits a compressive component tangent to the surface. Considering only the first quarter-wavelength of the R-wave and applying the maximum normal stress fracture criterion, where the crack propagation takes place perpendicular to the direction of the maximum principal stress, it is clear that the crack would grow into the material, in the direction opposite to that of R-wave propagation, at some angle from the vertical. But consideration of the second and third quarter-wavelengths of the R-wave, which seem to be the dominant portions, shows that the crack would grow into the material, away from the direction where the R-wave originated, at some angle from the vertical. The last quarter-wavelength could again cause the crack to change direction, but the magnitudes of the stresses would probably not support continued crack propagation. If a prediction were to be made of the final overall R-wave crack propagation length, it would be of the order of one-quarter of a wavelength. This assumes a crack to R-wave velocity ratio of one-third and that the crack would start propagating at a value of normalized distance along the surface, x/e , of 0.75.

Experimental results and comparison

The experimental model is shown in Figure 4. It consists of a $18 \times 24 \times 1/2$ inch plate of Homalite 100, a transparent, birefringent material which is homogeneous and isotropic. A micro-crack or flaw across the plate thickness was induced on the edge, by tapping an X-acto knife edge softly with a hammer. The micro-crack is 10 inches away from the

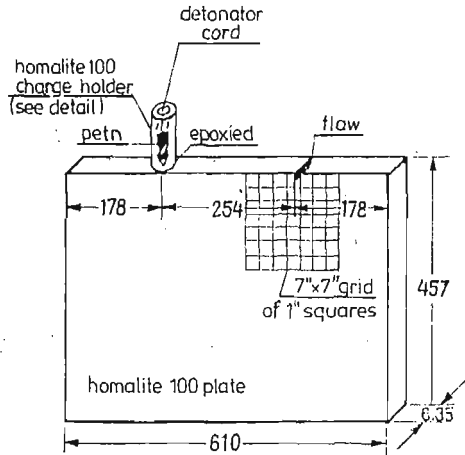


Fig. 4. The experimental model

Homalite 100 cylindrical charge holder 6,35mm — diameter \times 1" long), which was hollowed out with a 3,17mm diameter drill and epoxied on to the edge of the model plate. The explosive used was 200 mg of PETN. A 7" \times 7" grid of one-inch squares was drawn with black ink on the side of the Homalite 100 plate facing the camera. This experimental model is used to simulate, under controlled conditions, the extension of a surface micro-crack as the R-wave moves past it along the edge of the plate. Care was taken in choosing the size of the plate so as to prevent reflected stress waves from impinging upon the crack which would alter the results.

Using this experimental set-up several tests were run. A typical test is presented here and the results are compared to the theory. Figure 5 shows the isochromatic patterns associated with a R-wave moving from left to right, and the location and size of the initial crack. Notice that the leading fringes of the R-wave appear unaffected by the presence of the crack which has an initial length of 0,53 mm inches which corresponds to a length normalized with respect to the wavelength of 0,006. The initial normalized depth is less than that which Dally [8] found to have negligible effect on the R-wave characteristic

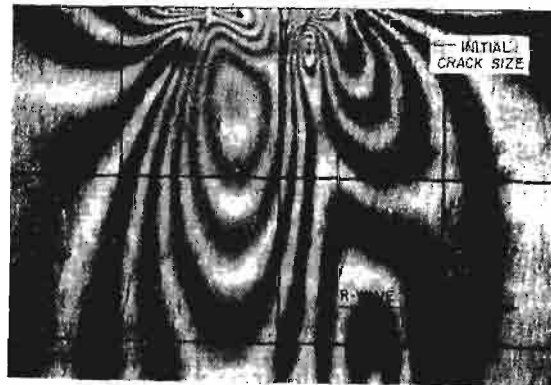


Fig. 5.

stress distribution, which was 0.018. Figure 6 shows the final crack size. It also shows some effects of R-wave component reflections as is evident from the jagged look of some of the isochromatic fringes. The crack in Figure 5 is located, with respect to the R-wave, at a fringe of order of 2.5 on the leading portion of the R-wave.

Figure 7 shows a comparison of the experimentally obtained isochromatics with the theoretical predictions using the Classical and Lamb solutions, for the plane stress case. The resemblance between the experimental and the Lamb solution result is very close. Therefore, the theoretical solution and the methods used to obtain it from the experimental result are adequate. This also implies that the description of the stresses in the entire R-wave field is being modelled correctly.

Figure 8 shows the experimental result as a composite of the crack tip location in each of the frames. As such, it incorporates a greater amount of experimental error because

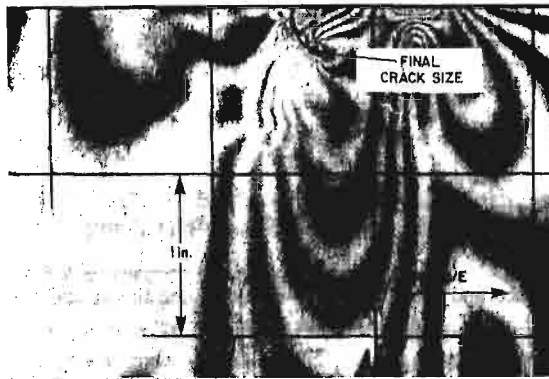


Fig. 6.

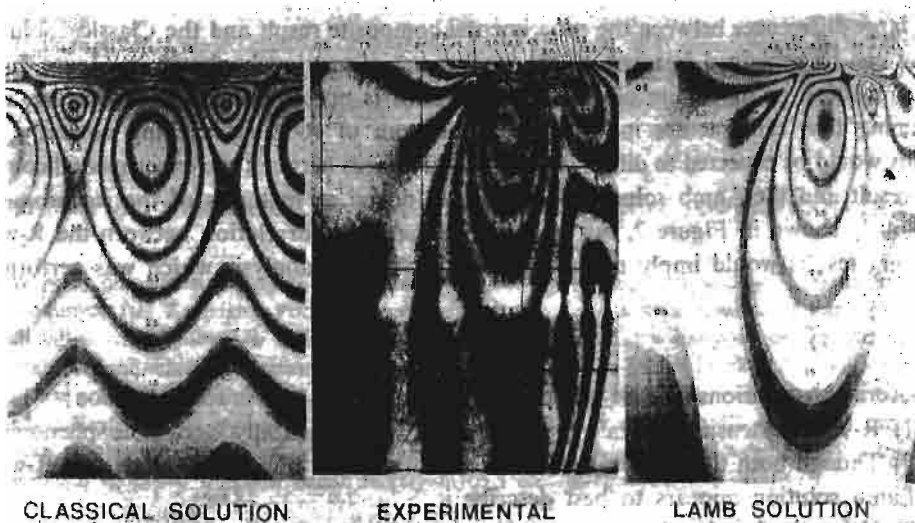


Fig. 7. A Comparison of the experimental and theoretical full-field isochromatic patterns: a) classical solution, b) experimental result, c) Lamb solution

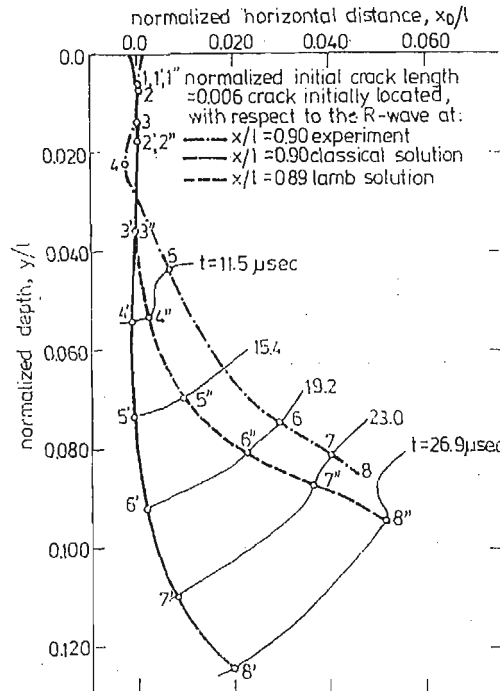


Fig. 8. A comparison in space and time of the experimental and theoretical results of crack extension induced by the Rayleigh wave

of the changing perspective in the Cranz-Schardin camera, since each frame has a separate lens location. Also plotted in Figure 8 are the predictions obtained using the Classical and Lamb solutions. Lines have been drawn in Figure 8 to show equal absolute times. The large differences between the experimental composite result and the Classical solution result can be explained in terms of the isochromatics previously shown in Figure 7, i.e., the simulation or modelling of the full stress field is not at all similar. Therefore, even assuming that the fracture models the phenomena of R-wave cracking correctly, the results would be expected to differ. The small differences between the experimental composite result and the Lamb solution can also be looked at in terms of the isochromatics previously shown in Figure 7, but in this case the close correlation between the R-wave cracking results would imply the validity of the fracture analysis which was performed.

Conclusions

Several observations can be made with regard to R-wave crack extension:

- (1) R-wave extension of micro-cracks is an experimentally verifiable phenomena.
- (2) Though both the Classical and Lamb solutions can be used to model the R-wave, the Lamb solution appears to best describe it.
- (3) Using the Lamb solution in combination with the Griffith-Irwin maximum strain energy release rate criterion it is possible to approximate R-wave micro-crack extension reasonably well.

Bibliography

1. J. F. GARDENAS-GARCIA, and D. C. HOLLOWAY, *Theoretical and Experimental Investigation of the Propagation of Surface Cracks by the Rayleigh Wave*, Proceedings of the Society for Experimental Stress Analysis Annual Spring Conference, Cleveland, Ohio, pp. 937 - 944, May 1983.
2. H. LAMB, *On the Propagation of Tremors over the Surface of an Elastic Solid*, Phil. Trans. Royal Soc., Vol. A203, pp. 1 - 42, 1904.
3. J. W. DALLY, and S. A. THAU, *Observations of Stress Wave Propagation in a Half-Plane with Boundary Loading*, International Journal of Solids and Structures, Vol. 3, pp. 293 - 308, 1967.
4. S. A. THAU, and J. W. DALLY, *Subsurface Characteristics of the Rayleigh Wave*, International Journal of Engineering Science, Vol. 7, pp. 37 - 52, 1969.
5. E. H. YOFFE, *The Moving Griffith Crack*, The Philosophical Magazine, Vol. 42, Seventh Series, No. 330 pp. 739 - 750, 1951.
6. A. A. GRIFFITH, *The Phenomenon of Rupture and Flow in Solids*, Philosophical Transactions of the Royal Society of London, Vol. A221, pp. 163 - 198, 1920.
7. G. R. IRWIN, *Fracture Dynamics*, Fracturing of Metals, American Society for Metals, p. 152, 1948.
8. J. W. DALLY, *Dynamic Photoelastic Studies of Stress Wave Propagation*, Modern Problems in Elastic Wave Propagation, J. Miklowitz and J. D. Achenbach (Eds.), John Wiley and Sons, Inc., New York (1978),

Резюме

ТЕОРЕТИЧЕСКИЕ И ЭКСПЕРИМЕНТАЛЬНЫЕ ИССЛЕДОВАНИЯ МИКРОТРЕЩИН
ВЫЗВАННЫХ ВОЛНАМИ РЭЛЕЙА

В работе обсуждены теоретические и экспериментальные исследования роста поверхностных микротрещин вызванных волной Рэлея.

Теоретический подход использует решение Лямба для пропагации поверхностной волны в двумерной однородной изотропной среде для случаев плоского поля напряжений и деформаций.

Применяя признак Гриффитса — Ирвина скорости освобождения энергии для трещин подверженных нагрузкам I и II типов, предусмотрено допустимую длину микротрещин вызванных волнами Рэлея.

В экспериментальном подходе применено фотоупругость для наблюдения распределения изохром связанных с пробегом волны Рэлея вдоль берега двупреломленного материала. Получено удовлетворительную сходимость теоретических и экспериментальных результатов.

Streszczenie

TEORETYCZNE I DOŚWIADCZALNE BADANIA MIKROPĘKNIĘĆ POWODOWANYCH FAŁĄ
RAYLEIGHA

W pracy omówiono teoretyczne i doświadczalne badania rozwoju mikropęknięć powierzchniowych powodowanych falą Rayleigha. Podejście teoretyczne wykorzystuje polowe rozwiązanie Lamba dla propagacji fali powierzchniowej w dwuwymiarowym ośrodku jednorodnym izotropowym, dla przypadków płaskiego pola naprężeń i odkształceń. Stosując kryterium Griffitha-Irwina prędkości zwolnienia energii dla pęknięć poddanych I i II typowi obciążeń, przewidywano drogę i długość mikropęknięć wywoływanych przez fale Rayleigha. W podejściu doświadczalnym stosowano elastooptykę dla obserwacji rozkładów izochrom związanych z przebiegiem fali Rayleigha wzdłuż brzegu materiału dwójłomnego. Otrzymano zadowalającą zgodność wyników badań teoretycznych i doświadczalnych.

Praca została złożona w Redakcji dnia 20 kwietnia 1985 roku